Valance Band states evolution in AlGaAs QDs systems in inverted pyramids

M. Lazarev[1,2], and E. Kapon[2]

[1]Department of Computer Science, LAMBDA, National Research University Higher School of Economics (HSE), Russia

[2]Laboratory of Physics of Nanostructures Ecole Polytechnique Fédérale de Lausanne (EPFL) Switzerland

Abstract

Metal Organic Vapor-Phase Epitaxy (MOVPE) growth in inverted pyramid provide opportunity to grow nanostructure with predictable heterostructure potential. In this paper we investigating the effect of nanostructure geometry and composition on optical properties and Valance Band (VB) character on example of single Quantum Dot (QD), Quantum Dot Molecules (QDMs) and QD superlattices. As a model structure we take well known explored Quantum Dots (QDs) GaAs/AlGaAs systems in inverted pyramids. We examine optical properties under external electric field and demonstrate dynamic way to control the optical polarization properties and its evolution. Another interesting effect is special modularity of the hole wavefunction also effects on its type. In case of strong modularity and even in long QD that Ground State (GS) of the VB may be turned from light hole to the heavy type. The ability to control the optical properties of QDs is important for fabrication of future nano-optical devices, since QDs are practical sources of single photons. In particular, the control over the energy and polarization of the emitted photons is important for quantum information technologies.

1. Introduction

Low dimensional nanostructures have been studding for a long time since 60th. Since then, techniques, material quality improved and number of available materials increased. Each family of nanostructures have its unique optical character influenced by geometry and composition. Such nanostructures found wide range of applications for example in solar cells [1], LEDs [2], lasers [3] and so on [4]. Dimensionality plays curtail role in light-matter interaction and charge carrier's properties, thus optical character of the nanostructure. In Quantum wells (QWs) light emission happens du to recombination of electrons with heavy holes [link] in opposition to Quantum Wires (QWRs) where electrons recombine with light holes. This difference has impact on emitted light polarization [link]. In contrast QDs have complex spectral structure where carrier states can be as heavy and light. In this paper we consider GaAs/AlGaAs nanostructures. Previously has been shown that the hole character (heavy or light) in the Valance Band (VB) in QD can be modified in variety of structures QDs[link] QDMs[link] and etc [link].

The ability to control the optical properties of QDs is important for fabrication of future nano-optical devices, since QDs are practical sources of single photons. In particular, the control over the energy and polarization of the emitted photons is important for quantum information technologies [link]. In this paper, we focus on dynamic ways to control the optical polarization properties of different nanostructure types realized by pyramidal heterostructures.

We study here theoretically the transition process between LH- and HH-like character for a pyramidal QD of different geometries. In this paper we use the same modeling approach as in [link]. The height t of the QD cylinder (the QD "thickness) is varied between 8 to 23 nm (see inset in Fig. 1(a)).

As a model structure we take QDs grown in inverted pyramids [link]. It's well studied experimentally and was demonstrates ability to control the structure composition and geometry with high precision of 1 nm. The MOVPE growth technique allows to grow all possible variety of nanostructures by control in heterostructure composition along the growth direction. The sample structures presented in figure 1. In this paper we will focus on single QDs (fig 1 b) QDM (fig 1 d) and QDSL (figure 1 f)

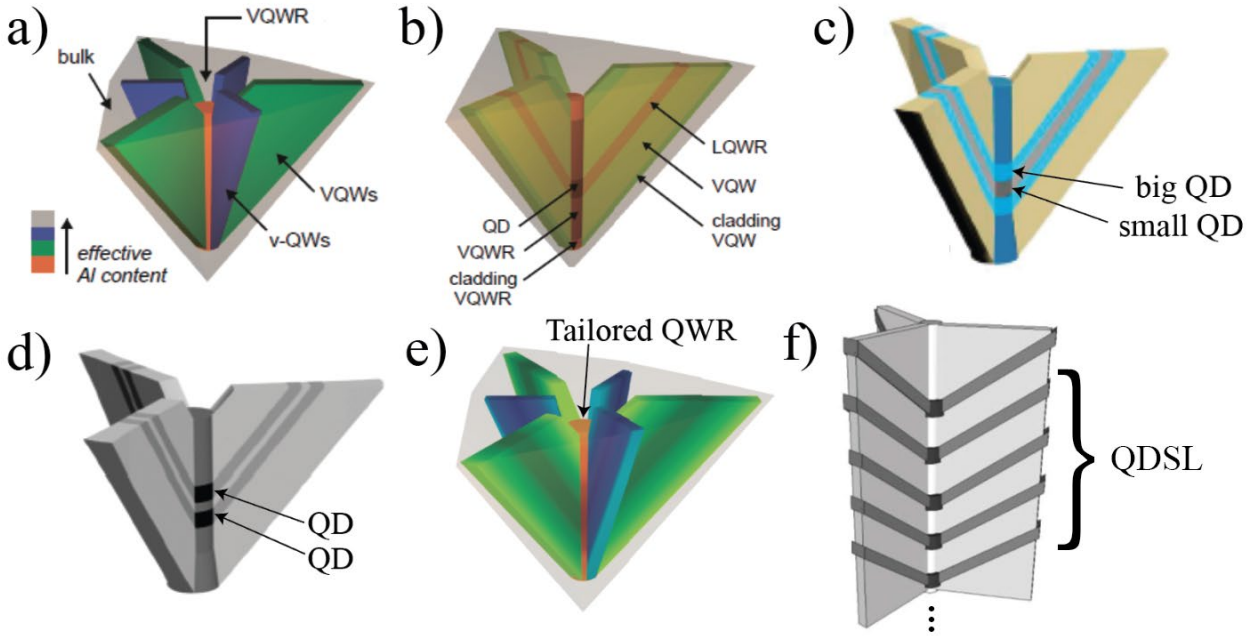

Figure 1. Schematic illustration of different kind of AlGaAs nanostructures embedded in inverted pyramids presented in this paper. (a) "Long" quantum wire (QWR) laterally bounded by "vertical" QWs, (b) parabolic potential quantum dot (PQD), and (c) QD-in-QWR heterostructure. (d)QDM of two coupled QDs (e)Tailored potential QWR/QD (f) QDSL of N coupled QDs. The color codes scales the Al mole fraction in the different parties of the heterostructures.

2. Model of confined states

We use the so-called mean field (Hartree-Fock) approximation. The result is a mean-field Hamiltonian for single electrons, $H = \frac{p^2}{2m_0} + V(r) + H_{SO}$ where *V(r)* is mean field potential, spin-orbit interaction term $H_{SO} = \frac{\hbar}{4m_0^2 c^2}\sigma \cdot \left[\nabla V \times p\right]$ and m_0 is the electron mass.

Exploiting the lattice periodicity, we first look for solutions in the form of Bloch waves:

$$\psi_k^{(n)}(r) = u_k^{(n)}(r)e^{ikr},\ u_k^{(n)}(r) = u_k^{(n)}(r+a)$$

Substituting the Bloch wave function into the Hamiltonian and neglecting parts with fast oscillations we get [5]: $H = H^{k\cdot p} + H_{SO}$, where $H^{k\cdot p} = \left[\frac{p^2}{2m_0} + V(r)\right] + \left[\frac{\hbar}{m_0} k\cdot p + \frac{\hbar^2 k^2}{2m_0}\right]$, thus the Schrödinger equation looks like:

$$\left(\left[\frac{p^2}{2m_0} + V(r)\right] + \left[\frac{\hbar}{m_0} k\cdot p + \frac{\hbar^2 k^2}{2m_0}\right] + \frac{\hbar}{4m_0^2 c^2}\sigma\cdot\left[\nabla V \times \left(p + \hbar k\right)\right]\right) u_k^{(n)}(r) = \varepsilon_k^{(n)} u_k^{(n)}(r)$$

Where σ are Paul matrixes, ∇V gradient of atomic mean field potential. Our model works with this Hamiltonian and solve it in 4-bands (S and P orbitals) approximation. To take into account infinite number of other bands Lowdin perturbation theory [6] was implied. The resalting Hamiltonian in matrix form taking in to account SO interaction looks like: $H = H_0 + H' + H^{SO}$ where:

$$H_0 = \begin{pmatrix}
E_C+\varepsilon & iP_0k_x & iP_0k_y & iP_0k_z & 0 & 0 & 0 & 0 \\
-iP_0k_x & E_V+\varepsilon & 0 & 0 & 0 & 0 & 0 & 0 \\
-iP_0k_y & 0 & E_V+\varepsilon & 0 & 0 & 0 & 0 & 0 \\
-iP_0k_z & 0 & 0 & E_V+\varepsilon & 0 & 0 & 0 & 0 \\
0 & 0 & 0 & 0 & E_C+\varepsilon & iP_0k_x & iP_0k_y & iP_0k_z \\
0 & 0 & 0 & 0 & -iP_0k_x & E_V+\varepsilon & 0 & 0 \\
0 & 0 & 0 & 0 & -iP_0k_y & 0 & E_V+\varepsilon & 0 \\
0 & 0 & 0 & 0 & -iP_0k_z & 0 & 0 & E_V+\varepsilon
\end{pmatrix}$$

$$H^{SO} = \frac{\Delta_0}{3}\begin{pmatrix}
0 & 0 & 0 & 0 & 0 & 0 & 0 & 0 \\
0 & 0 & -i & 0 & 0 & 0 & 0 & +1 \\
0 & +i & 0 & 0 & 0 & 0 & 0 & -i \\
0 & 0 & 0 & 0 & 0 & -1 & +i & 0 \\
0 & 0 & 0 & 0 & 0 & 0 & 0 & 0 \\
0 & 0 & 0 & -1 & 0 & 0 & +i & 0 \\
0 & 0 & 0 & -i & 0 & -i & 0 & 0 \\
0 & +1 & +i & 0 & 0 & 0 & 0 & 0
\end{pmatrix}$$

$$\varepsilon = \frac{\hbar^2 k^2}{2m_0}$$

$$H' = \begin{pmatrix}
0 & 0 & 0 & 0 & 0 & 0 & 0 & 0 \\
0 & +L'k_x^2 + Mk_y^2 + Mk_z^2 & N'k_xk_y & N'k_xk_z & 0 & 0 & 0 & 0 \\
0 & N'k_yk_x & Mk_x^2 + L'k_y^2 + Mk_z^2 & N'k_yk_z & 0 & 0 & 0 & 0 \\
0 & N'k_zk_x & N'k_zk_y & Mk_x^2 + Mk_y^2 + L'k_z^2 & 0 & 0 & 0 & 0 \\
0 & 0 & 0 & 0 & 0 & 0 & 0 & 0 \\
0 & 0 & 0 & 0 & 0 & +L'k_x^2 + Mk_y^2 + Mk_z^2 & N'k_xk_y & N'k_xk_z \\
0 & 0 & 0 & 0 & 0 & N'k_yk_x & Mk_x^2 + L'k_y^2 + Mk_z^2 & N'k_yk_z \\
0 & 0 & 0 & 0 & 0 & N'k_zk_x & N'k_zk_y & Mk_x^2 + Mk_y^2 + L'k_z^2
\end{pmatrix}$$

A', *B*, *L*', *M*, *N*' are second order interactions due to Löwdin renormalization involving states outside the S, P subspace. $\varepsilon = \frac{\hbar^2 k^2}{2m_0}$ and Δ_0 is the spin-orbit splitting: $\Delta_0 = \frac{-3i\hbar}{4m_0c^2}\left\langle X\left|\frac{\partial V}{\partial x}p_y - \frac{\partial V}{\partial y}p_x\right|Y\right\rangle$. In case of GaAs, B=0.

This Hamiltonian contain 4 atomic bands, kinetic, spin-orbit, perturbation of 5 next bands and atomic potential in terms of mean field. Because transition rate is proportional to $\left\langle\varphi_{cb}\left|e\cdot p\right|\varphi_{vb}\right\rangle$ where *P* is momentum *e* is a polarization vector. For optical studies it's more convenient to change the basis of this Hamiltonian to the basis of eigenfunctions of momentum operator (HH and LH basis). Set of new basis wavefunction are presented in following table 1[link].

Eigenvalues and corresponding eigenstates at $\mathbf{k} = 0$.

Energy	First Kramers Set	Second Kramers Set	Name
E_c	$\left\|\frac{1}{2},-\frac{1}{2}\right\rangle = \left\|S\downarrow\right\rangle$	$\left\|\frac{1}{2},\frac{1}{2}\right\rangle = \left\|S\uparrow\right\rangle$	Electron
E'_v	$\left\|\frac{3}{2},\frac{3}{2}\right\rangle = \frac{i}{\sqrt{2}}\left\|(X+iY)\uparrow\right\rangle$	$\left\|\frac{3}{2},-\frac{3}{2}\right\rangle = \frac{-i}{\sqrt{2}}\left\|(X-iY)\downarrow\right\rangle$	Heavy Hole
E'_v	$\left\|\frac{3}{2},\frac{1}{2}\right\rangle = \frac{-i}{\sqrt{6}}\left\|(X+iY)\downarrow -2Z\uparrow\right\rangle$	$\left\|\frac{3}{2},-\frac{1}{2}\right\rangle = \frac{i}{\sqrt{6}}\left\|(X-iY)\uparrow +2Z\downarrow\right\rangle$	Light Hole
$E'_v-\Delta_0$	$\left\|\frac{1}{2},\frac{1}{2}\right\rangle = \frac{-i}{\sqrt{3}}\left\|(X+iY)\downarrow +Z\uparrow\right\rangle$	$\left\|\frac{1}{2},-\frac{1}{2}\right\rangle = \frac{-i}{\sqrt{3}}\left\|(X-iY)\uparrow -Z\downarrow\right\rangle$	SO Hole

Table 1 Eigenvalues and corresponding eigenstates of the CB and VB states.

New matrix elements in this basis looks like:

$$H_0 = \begin{pmatrix} E_c+\varepsilon & 0 & V & 0 & \sqrt{3}V^* & -\sqrt{2}U & -U & \sqrt{2}V \\ 0 & E_c+\varepsilon & -\sqrt{2}U & -\sqrt{3}V & 0 & -V^* & \sqrt{2}V^* & U \\ V^* & -\sqrt{2}U^* & E_V & 0 & 0 & 0 & 0 & 0 \\ 0 & -\sqrt{3}V^* & 0 & E_V & 0 & 0 & 0 & 0 \\ \sqrt{3}V & 0 & 0 & 0 & E_V & 0 & 0 & 0 \\ -\sqrt{2}U^* & -V & 0 & 0 & 0 & E_V & 0 & 0 \\ -U^* & \sqrt{2}V & 0 & 0 & 0 & 0 & E_V & 0 \\ \sqrt{2}V^* & U^* & 0 & 0 & 0 & 0 & 0 & E_V \end{pmatrix}$$

$$H^{SO} = \frac{\Delta_0}{3}\begin{pmatrix} 0 & 0 & 0 & 0 & 0 & 0 & 0 & 0 \\ 0 & 0 & 0 & 0 & 0 & 0 & 0 & 0 \\ 0 & 0 & 1 & 0 & 0 & 0 & 0 & 0 \\ 0 & 0 & 0 & 1 & 0 & 0 & 0 & 0 \\ 0 & 0 & 0 & 0 & 1 & 0 & 0 & 0 \\ 0 & 0 & 0 & 0 & 0 & 1 & 0 & 0 \\ 0 & 0 & 0 & 0 & 0 & 0 & -2 & 0 \\ 0 & 0 & 0 & 0 & 0 & 0 & 0 & -2 \end{pmatrix}$$

$$H' = \begin{pmatrix} 0 & 0 & 0 & 0 & 0 & 0 & 0 & 0 \\ 0 & 0 & 0 & 0 & 0 & 0 & 0 & 0 \\ 0 & 0 & -P+Q & -S^* & R & 0 & \sqrt{3/2}S & -\sqrt{2}Q \\ 0 & 0 & -S & -P-Q & 0 & R & -\sqrt{2}R & \sqrt{1/2}S \\ 0 & 0 & R^* & 0 & -P-Q & S^* & \sqrt{1/2}S^* & \sqrt{2}R^* \\ 0 & 0 & 0 & R^* & S & -P+Q & \sqrt{2}Q & \sqrt{3/2}S^* \\ 0 & 0 & \sqrt{3/2}S^* & -\sqrt{2}R^* & \sqrt{1/2}S & \sqrt{2}Q & -P & 0 \\ 0 & 0 & -\sqrt{2}Q & \sqrt{1/2}S^* & \sqrt{2}R & \sqrt{3/2}S & 0 & -P \end{pmatrix}$$

Where: $\varepsilon = \frac{\hbar^2 k^2}{2m_0}, U = \frac{P_0}{\sqrt{3}}k_z, V = \frac{P_0}{\sqrt{6}}(k_x + ik_z), P = \frac{\hbar^2}{2m_0}\gamma_1\left(k_x^2+k_y^2+k_z^2\right),$

$$Q = \frac{\hbar^2}{2m_0}\gamma_2\left(k_x^2+k_y^2-2k_z^2\right),\ S = 2\sqrt{3}\frac{\hbar^2}{2m_0}\gamma_3\left(k_xk_z - ik_yk_z\right), R = -\sqrt{3}\frac{\hbar^2}{2m_0}\left(\gamma_2\left(k_x^2-k_y^2\right) - 2i\gamma_3k_xk_y\right),$$

$$\gamma_1 = -\frac{2}{3}\frac{m_0}{\hbar^2}\left(L'+2M\right)-1\ ,\gamma_2 = -\frac{1}{3}\frac{m_0}{\hbar^2}\left(L'-M\right),\ \gamma_3 = -\frac{1}{3}\frac{m_0}{\hbar^2}N'.$$

By dashed lines, we separate valence band of the Hamiltonian from coupled conduction band part. Where Δ is spin-orbit splitting and $\gamma_1,\gamma_2,\gamma_3$ is Luttinger parameters. In the case of GaAs $\gamma_1 = 6.98$ $\gamma_2 = 2.06$ $\gamma_3 = 2.93$ [7]. In constant media Luttinger parameters does not depend of coordinates, in GaAs media case effective masses of light and heavy holes depends of direction of holes propagation. In case of $Al_xGa_{1-x}As$ Luttinger parameters are chosen as linearly interpolation between the GaAs and AlAs. In AlAs Luttinger parameters are $\gamma_1 = 3.76$ $\gamma_2 = 0.82$ $\gamma_3 = 1.42$.

The Luttinger Hamiltonian that we discased so far is written in the x, y and z directions correspond to the principal crystallographic directions [hhe]. In this paper we consider structures with modulated potential along z [111] direction, thus the Hamiltonian needs to be rewritten to a new basis. Since SO and CB bands are far from LH and HH for simplicity we decouple them. Thus, 3D Schrodinger equation with effective mass for conduction band electrons can be solved separately from Luttinger Hamiltonian for VB. The Luttinger Hamiltonian in new basis looks like [link]:

$$H = \begin{bmatrix} D_{HH} & -S & R & 0 \\ -S^{\dagger} & D_{LH} & 0 & R \\ R^{\dagger} & 0 & D_{LH} & S \\ 0 & R^{\dagger} & S^{\dagger} & D_{HH} \end{bmatrix}$$

$$D_{HH} = -\frac{\hbar}{2m_e}\left[\frac{\partial}{\partial x}(\gamma_1+\gamma_3)\frac{\partial}{\partial x}+\frac{\partial}{\partial y}(\gamma_1+\gamma_3)\frac{\partial}{\partial y}+\frac{\partial}{\partial z}(\gamma_1-2\gamma_3)\frac{\partial}{\partial z}\right]+V$$

$$D_{LH} = -\frac{\hbar}{2m_e}\left[\frac{\partial}{\partial x}(\gamma_1-\gamma_3)\frac{\partial}{\partial x}+\frac{\partial}{\partial y}(\gamma_1-\gamma_3)\frac{\partial}{\partial y}+\frac{\partial}{\partial z}(\gamma_1+2\gamma_3)\frac{\partial}{\partial z}\right]+V$$

$$R = \frac{\hbar}{2m_e}\sqrt{3}\left[\frac{\partial}{\partial x}\left(\frac{2\gamma_3+\gamma_2}{3}\right)\frac{\partial}{\partial x}-\frac{\partial}{\partial y}\left(\frac{2\gamma_3+\gamma_2}{3}\right)\frac{\partial}{\partial y}-i\frac{\partial}{\partial x}\left(\frac{2\gamma_3+\gamma_2}{3}\right)\frac{\partial}{\partial y}-i\frac{\partial}{\partial y}\left(\frac{2\gamma_3+\gamma_2}{3}\right)\frac{\partial}{\partial x}\right]$$
$$+\frac{\hbar}{m_e}\frac{2}{\sqrt{6}}\left[\frac{\partial}{\partial x}(\gamma_3-\gamma_2)\frac{\partial}{\partial z}+\frac{\partial}{\partial z}(\gamma_3-\gamma_2)\frac{\partial}{\partial x}+i\frac{\partial}{\partial y}(\gamma_3-\gamma_2)\frac{\partial}{\partial z}+i\frac{\partial}{\partial z}(\gamma_3-\gamma_2)\frac{\partial}{\partial y}\right]$$

$$S = -\frac{\hbar}{2m_e}\sqrt{3}\left[\frac{\partial}{\partial x}\left(\frac{\gamma_3+2\gamma_2}{3}\right)\frac{\partial}{\partial z}+\frac{\partial}{\partial z}\left(\frac{\gamma_3+2\gamma_2}{3}\right)\frac{\partial}{\partial x}-i\frac{\partial}{\partial y}\left(\frac{\gamma_3+2\gamma_2}{3}\right)\frac{\partial}{\partial z}-i\frac{\partial}{\partial z}\left(\frac{\gamma_3+2\gamma_2}{3}\right)\frac{\partial}{\partial y}\right]$$
$$-\frac{\hbar}{2m_e}\sqrt{\frac{2}{3}}\left[\frac{\partial}{\partial x}(\gamma_3-\gamma_2)\frac{\partial}{\partial x}-\frac{\partial}{\partial y}(\gamma_3-\gamma_2)\frac{\partial}{\partial y}+i\frac{\partial}{\partial x}(\gamma_3-\gamma_2)\frac{\partial}{\partial y}+i\frac{\partial}{\partial y}(\gamma_3-\gamma_2)\frac{\partial}{\partial x}\right]$$

To Each pair of electron and hole corresponds exciton energy and definer as follows:

$$E_X = E_g + E_{cb} + E_{vb} - E_{Coulomb}^{e-h}$$

Where E_{cb} and E_{vb} confinement energies of CB and VB. As a conscience the exciton energy depends on the confinement potential of the nanostructure. Thus QDs, the excitonic structure depends on the relative size of quantum confinement energy and the electron-hole Coulomb energy. Usually in small QDs confinement is strong compared to the Coulomb interaction. Thus, exciton spectra are dominated not by Coulomb interaction as in bulk or QWs but by QD single-particle energy levels structure. The Coulomb interaction in the case of strong confinement can be considered as a perturbation [8]. The perturbation Hamiltonian is then written as:

$$E_{Coulomb}^{e-h} = \iint \psi_{cb}\psi_{vb}\frac{e^2}{4\pi\varepsilon_0\varepsilon|r_{cb}-r_{vb}|}\psi_{cb}^{*}\psi_{vb}^{*}dr_{cb}dr_{vb}$$

where ψ_{vb}, ψ_{cb} are the valence and conduction band wavefunctions, r_{cb}, r_{vb} the electron and hole positions. This approach is applied to the pyramidal QDs investigated in this paper.

Observed light intensity and polarization dependence proportional to dipolar momentum matrix element [link]:

$$I_{\mathrm{eh}} = \sum_{s_z=\pm\frac{1}{2}} \left| \sum_{j_z=\pm\frac{3}{2},\pm\frac{1}{2}} \langle \phi_{\mathrm{e}}^{s_z}(\mathbf{r}) | \phi_{\mathrm{h}}^{j_z}(\mathbf{r}) \rangle \langle u_{\mathrm{e}}^{s_z} | \mathbf{e} \cdot \mathbf{p} | u_{\mathrm{h}}^{j_z} \rangle \right|^2$$

Where $\boldsymbol{e}$ is polarization $\boldsymbol{p}$ is momentum operator $\boldsymbol{u}$ is Bloch wavefunction. The identical polarization dependence corresponds to photon from electron hole recombination in exciton. The final expression for polarization dependence in case of orthogonal LH and HH wavefunctions along and perpendicular z direction is:

$$I_z \propto \left(\frac{4}{3} \langle \varphi_e | \varphi_{LH} \rangle^2 \right) I_{xy} \propto \left(\langle \varphi_e | \varphi_{HH} \rangle^2 + \frac{1}{3} \langle \varphi_e | \varphi_{LH} \rangle^2 \right)$$

The model code is available on Github: *https://github.com/Mikelazarev/Low-dimensional-band-structure-model-*

The code contains a model in with heterostructure can be set layer by layer with any grid size. To model heterostructures in inverted pyramids the actual material distribution and geometry parameters have to be taken [link]. The actual parameters can be taken for previous studies [link][link][link] taking in to account segregation and nanocapillary effects. The pyramid geometry is already implemented in the code but that does not limit the model since it is possible to set any 3d structure. As well as for materials you can use to model InGaAs nanostructures as well. Note that InGaAs it is material with strain and the Hamiltonian presented above have to be modified for strained material.

In this paper we study here theoretically LH- and HH-like VB evolution for a pyramidal QD systems from its geometry and material composition (potential profile). The example of the model structure geometry is presented in figure 2 10 nm thick GaAs QD imbedded in AlGaAs barriers. The modeled aria is 40x40 nm size is enough to make sure that border conditions (infinite barriers) do not have effect on exciton structure in the aria of interest. The geometry details and ratio of material distribution in different modeled aria parts is well described in previous study [link][link]. Figure 2 b illustrates Al distribution in ZX plane (Y~0). Here we will just remind the main numbers. The actual Al content in the core cylinder of the QD is 0%, and that in the vertical barrier cylinders it is ~5% (for 40% nominal Al content). Each 1% of Al content gives ~13 meV to the band gap. The ratio between the CB and VB offsets was taken as ΔCB/ ΔVB ~67/33[9][10]. The diameter of the QD/QWR cylinders is kept at 18 nm. The bandgap dependence over Al content in GaAs is known from the literature [7]:

$$E_g\left(Al_xGa_{1-x}As\right) = (1-x)E_g\left(GaAs\right) + xE_g\left(AlAs\right) - x(1-x)C\,.$$

where C is the bowing parameter, $E_g(GaAs)$= 1.519 eV and $E_g(AlAs)$= 3.1 eV (low temperature values).

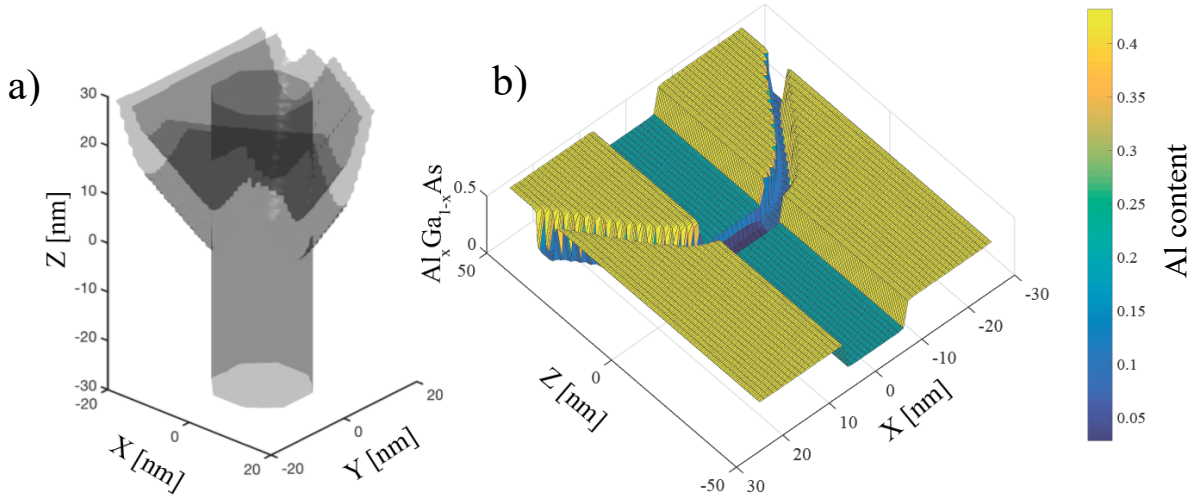

Figure 2. (a) 3D isosurface of Al content (x=0.4) in a simulated 10 nm thick GaAs QD nanostructure. (b) Z-X cut of the simulated nanostructure showing Al content distribution.

3. Results and discussion

3.1 LH and HH states evolution in QD

Figure 3 presents the calculated confinement energies of the lowest CB and VB states versus the QD thickness *t*, without Coulomb interaction. The height t of the QD cylinder (the QD "thickness) is varied between 8 to 23 nm (see inset in Fig. 3(a)). The actual Al content in the core cylinder of the QD is ~1% (for 20% nominal Al content), and that in the vertical barrier cylinders it is ~5% (for 40% nominal Al content), it is illustrated in figure 3 (e) as dark and light region in vertical wire region (pyramid center). Remarkably, the LH- and HH- states cross in energy, for QD thickness t~ 12 nm (figure 3 (b). For t < 12 nm, the ground state is HH-like and the structure behaves in his respect as a "thin" QD. For t > 12 nm, the ground state is LH-like and the structure behaves as a QWR or elongated QD. These results suggest the choice of QD parameters for achieving a structure at the border between HH- and LH- behavior of the VB ground state.

The calculated polarization-resolved optical spectra of this QD structure are shown in figure 3 (a) for various thicknesses *t*; red and blue curves correspond to linear polarization normal and parallel to the growth direction. Line broadening of 2 meV was applied and Coulomb interaction was taken into account as a perturbation. From this set of spectra, we see the GS transition changes its character from LH to HH with reduction of QD thickness. Plotting the transition energies versus *t* (figure 3 (b)), we see that this transition happens for *t* between 12 and 14 nm. This transition also shows up in the VB mixing characteristic. Figure 3 (c) shows the HH and LH portions of the lowest VB states portions. Interestingly, the switching from HH to LH –like lowest energy state occurs near t=12 nm (as in figure 3(b)), different than for the switching thickness for the optical spectra due to the present's coulomb interaction.

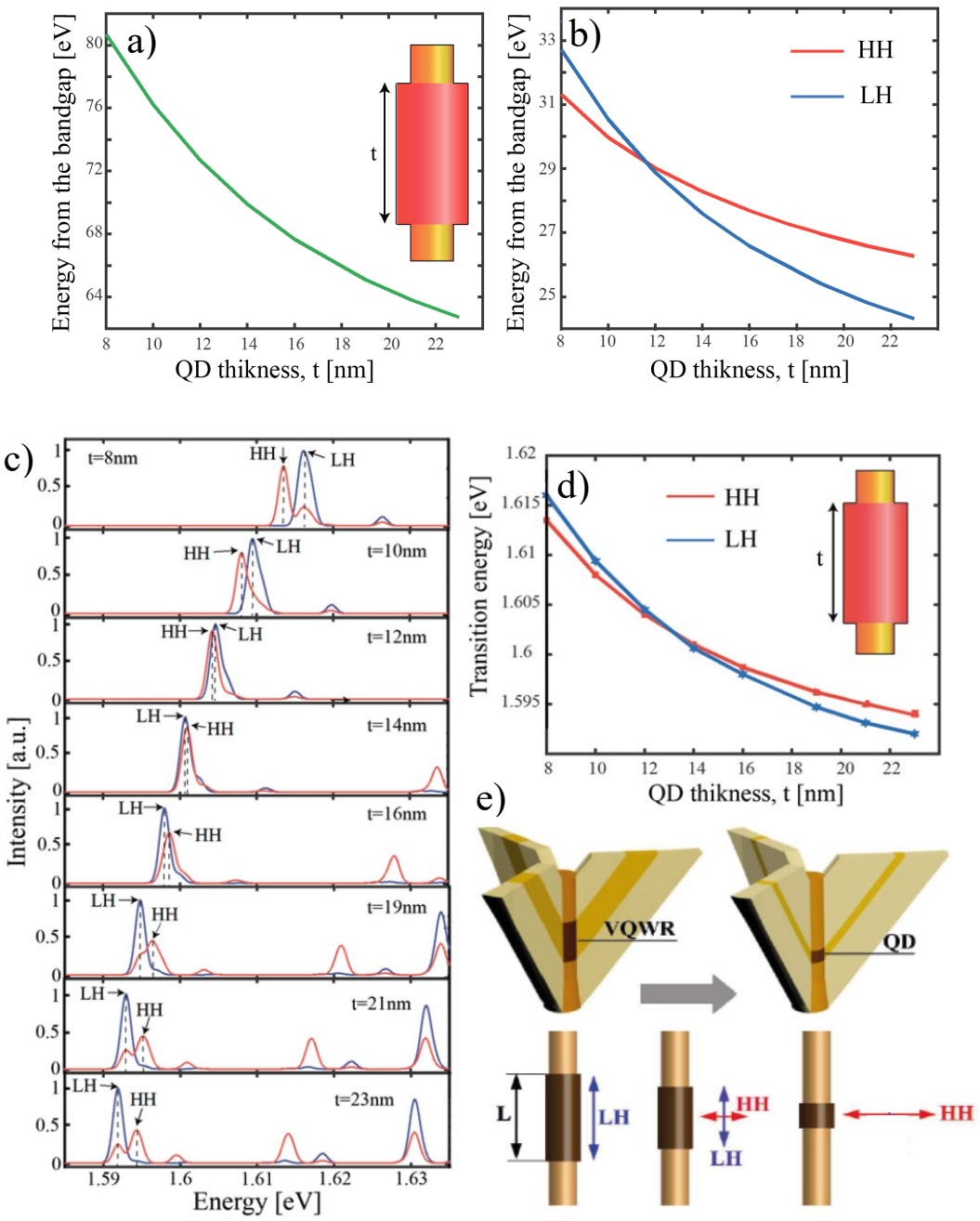

Figure 3 (a) Calculated dependence of energy of first CB state from QD thickness. (b) Calculated dependence of energy of first 2 VB state from QD thickness. Blue colors correspond to LH transitions, red to HH transition. (c) Calculated spectra of t=8 nm, 10 nm, 12 nm, 14 nm, 16 nm, 19 nm, 21 nm, 23 nm, QD thickness. Different colors correspond different polarizations, blue emission polarized in Z direction and red in XY plane. (d) Calculated energy of first 2 transitions from QD thickness. Different colors correspond to different transition type, the red color is CB and HH transition, blue color CB and LH transition. (e) Schematic illustration of QD in inverted pyramid.

We see that in a range of t=12-14 nm, the QD GS transition changes its polarization with the switching of the VB ground state character from LH to HH. Since, around this point, small variations in the confinement potential can yield such switching, such QD can serve as a base for

achieving the desired change using an electric field. Here we analyze the effect of an electric field on such “equilibrium”: QD structure.

To illustrate the effect of an electric field, we consider the same QD structure discussed above, and fix the QD thickness at t=14 nm. The confined CB and VB states are then computed with the addition of an electric field E oriented in the growth direction z. We note the absence of reflection symmetry of the pyramidal.

In figure 4 (a) shows the calculated optical spectra of the QD structure for an electric field of amplitude E=20000 V/cm, oriented along the growth direction. Comparing to the spectrum for E=0 (figure 2), we notice two major differences. First, the absorption edge is red shifted, which is due to a quantum confined Stark effect [170]. Secondly, lowest energy transition line with nearly equal LH and HH components develops for E>0 into a richer structure with characteristic polarization features. This is further illustrated by the DOLP spectrum, which shows a HH-like feature at low energies instead of DOLP~0 for E=0. This is because the E-field changes the QD potential profile such that the lowest VB state is HH-like and the Stark shifts are different for the different VB states. Thus, the application of an electric field can dynamically tune the QD structure so as to switch the polarization state of light emitted by the QD ground states. The impact of the E-field on the lowest transition states energy is displayed on the right panel of figure 4. The spectral lines near 1.595eV in figure 4 are related to the CB1-VB1 and CB1-VB2 transitions. Note that the polarization is determined by the portion of the VB wavefunction that best overlaps with the CB state.

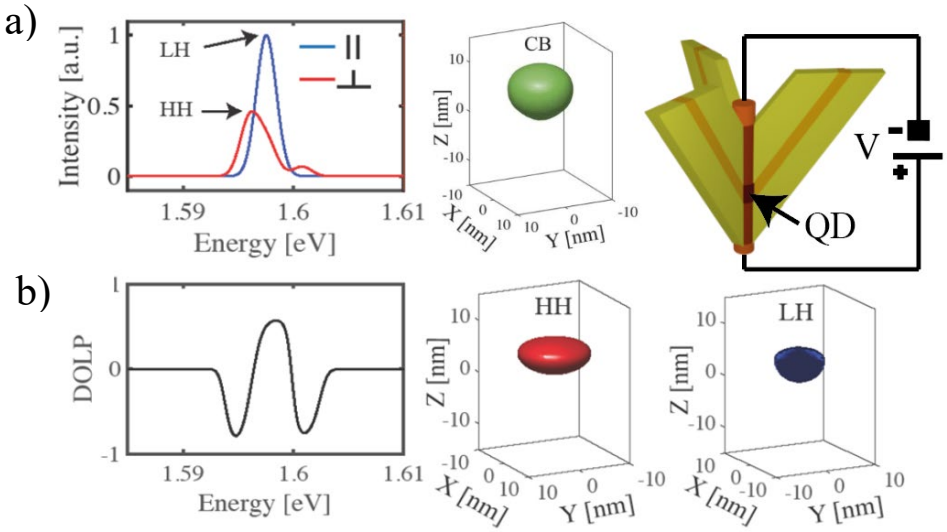

Figure 4. QD (t=14 nm), subject to an electric field E=20000 V/cm, applied in the z direction. Left panel: (a) Calculated optical spectra taking into account Coulomb interaction and 2 meV broadening. (b) DOLP spectra. Right panel: schematic presentation of QD in inverted pyramid with electric contact and wavefunction iso-surfaces of the two lowest energy CB and VB states: green – electron; red – HH; blue - LH.

3.2 QDM Polarization control by barrier adjustment

Here, we show the effect of barrier height on the polarization switching of the QDM GS emission. Figure 5 presents the dependence of the lowest CB and VB states on the nominal Al content in the outer barrier (nominal Al content in QD core: 20%; in external barriers: 40%, QD thickness t=7 nm; barrier thickness d=5 nm). The GS of the CB increases with increasing Al content, as the potential energy of the barrier increases. The VB states dependence is more complex: in between the two extreme barrier heights the VB GS changes its character from LH- to HH- like with increasing barrier height (see figure 5 b).

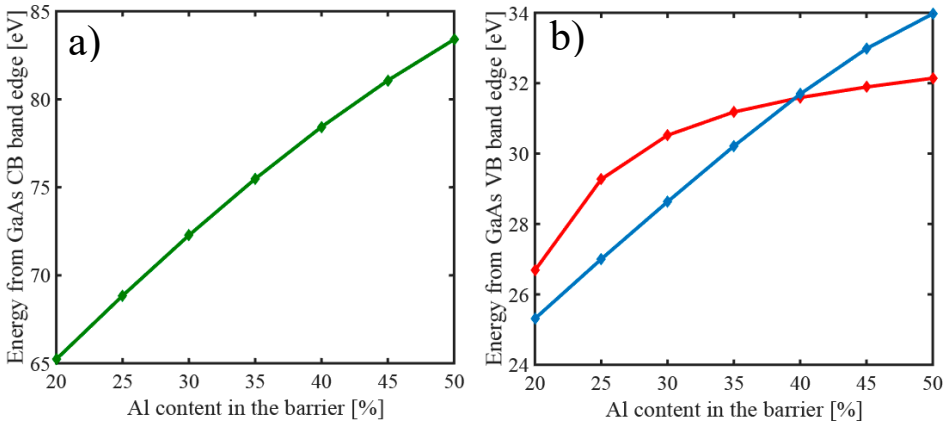

Figure 5 (a) Calculated confinement energy dependence of the first CB state versus the QDM barrier composition. Inset is schematic of the QDM core part. (b) Calculated energy position of the first 2 VB state from QD barrier composition. Blue line corresponds to LH transitions, red to HH transition.

Figure 6 (a) displays a summary of the calculated optical spectra, taking into account Coulomb interaction as a perturbation and a line broadening of 2 meV. The lowest energy transition is mainly LH-like for low barriers, and becomes degenerate with the HH-like one at ~40% Al. The spectra show the evolution of the HH and LH transition lines, their crossing when Al content becomes ~40%, and at 50% the complete change of the GS to HH one. Figure 6 (b) shows the spectral positions of the GS and the first excited transition versus the barrier Al content, indicating the VB character (red color for HH, blue for LH). Figure 6 (c) shows the VB mixing dependence on the barrier height. Summarizing, the common trend for all structures is that at certain vertical confinement strength the GS transition changes between LH to HH like, and as a consequence the emission polarization of the GS also changes. This figure illustrates the two regimes of behavior, with two different GS transition types and polarization of emitted light. The QDM system at the intermediate point were the HH and LH states are almost degenerate opens an opportunity to change dynamically the GS emission character by applying an external electric field, due to the sensitivity of such structure.

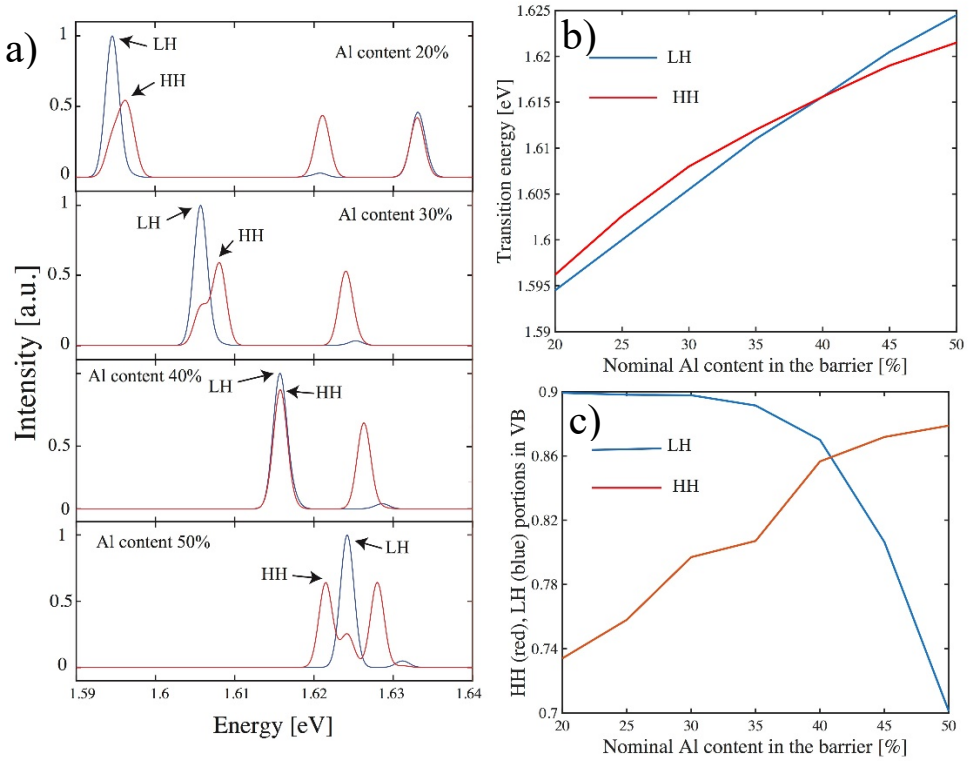

Figure 6 (a) Calculated polarization-resolved spectra of the QDM for different heights of the barrier (Al content). Blue and red curves correspond to linear polarization parallel and perpendicular to the growth directions. Coulomb interaction and linewidth broadening accounted for as in Chapter 4. Lines corresponding to HH-like and LH-like transitions are indicated. (b) Calculated energies of the lowest energy transitions in (a) versus QDM thickness barrier height. Different colors correspond to different transition types, the red line between CB and HH transition, blue line between CB and LH transition. (c) HH and LH portions in VB states presented in (b).

We consider the effect of an external electric field in a QDM with the following structural parameters: QD cores of 20% Al content and thickness t=7 nm each, QD external barriers of 40% Al content, QD inner barrier thickness d=5 nm and 35% Al content. Figure 7 shows the simulation results of the system without external electric field (*E=0*). Figure 7 (a) presents the calculated optical spectra and figure 7 (b) the corresponding DOLP spectra. For this configuration. The GS LH and HH transition are almost at the same energy, with more complex structure of the excited states transitions. The right panel of figure 7 shows side view of the lowest CB and VB states WFs isosurfaces.

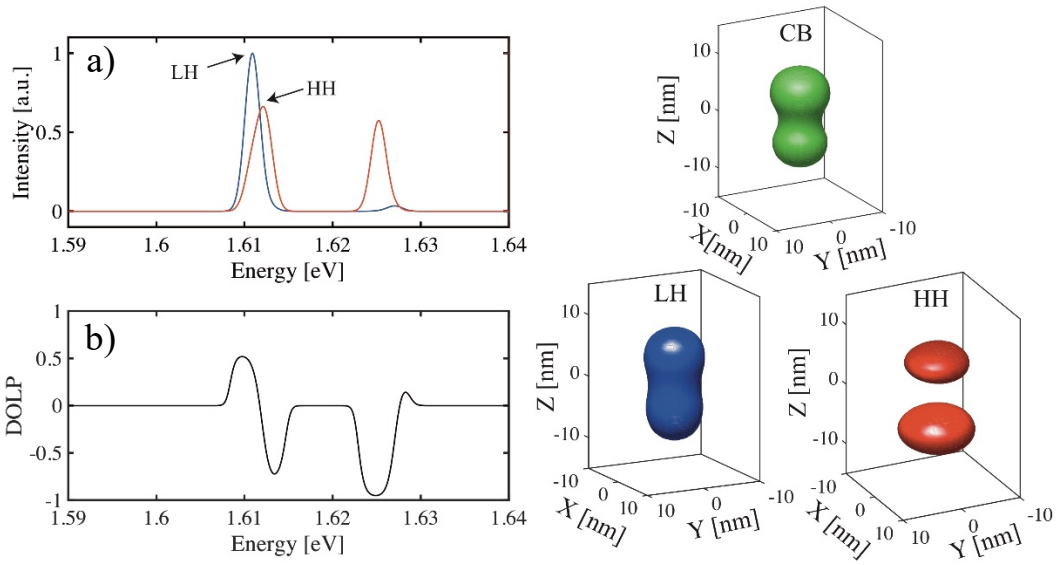

Figure 7 QDM structure (see text for parameters) without electric field. Left panel: (a) Calculated optical spectra taking into account Coulomb interaction and 2 meV broadening. (b) DOLP spectra. Right panel: wavefunction iso-surfaces of the lowest energy CB and VB states: green – electron; red – HH; blue - LH.

For the same QDM structure, the additional potential asymmetry induced by an external electric field of E=9000 [V/cm] aligned in the growth direction dramatically changes the optical spectra and WFs shapes (figure 8). As in the case of the single QD with the applied electric field, the polarization of the GS transition and its energy change. In contrast to the case E=0, the lowest energy transition has now DOLP=-0.6 as opposed to DOLP=+0.5 to its more important HH character of the VB state involved. Note that the CB and VB WFs are pushed in the opposite direction by the electric field, as usual for a Stark effect. This also leads to a reduction in the transition strength due to the smaller WF overlaps.

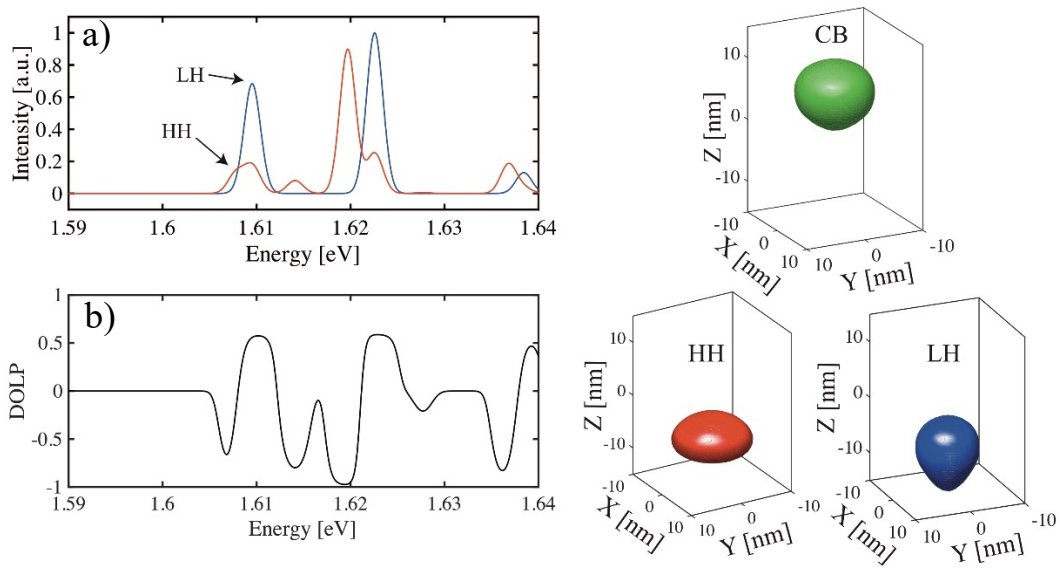

Figure 8 QDM structure (see text for parameters) subject to an electric field E=9000 V/cm, applied in the +z direction. Left panel: (a) Calculated optical spectra taking into account Coulomb

interaction and 2 meV broadening. (b) DOLP spectra. Right panel: wavefunction iso-surfaces of the lowest energy CB and VB states: green – electron; red – HH; blue – LH.

3.3 N coupled QS systems, QD superlattice.

A next step to scale up the family of nanostructures discussed is the formation of a QD superlattice (QDSL). QDSLs are useful for achieving entangled QD states and performing quantum manipulations of their WF features. In this section, we will consider QDSL structures formed in inverted pyramids, as shown schematically in figure 9. Using numerical simulations, we first demonstrate the formation of QDSL minibands and then introduce the effect of an applied electric field. The impact on the polarization of the emitted light is discussed.

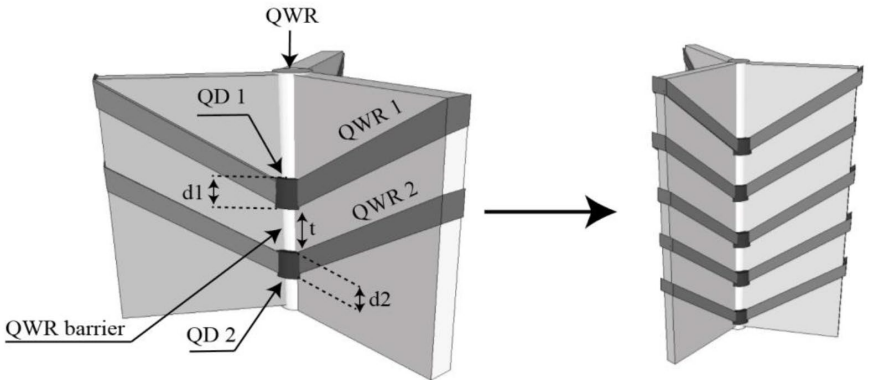

Figure 9. Schematic picture of pyramidal QD molecule (left) and pyramidal QD superlattice (right).

QDSLs can be realized experimentally in pyramidal systems as a vertically aligned coupled QD array. In such systems, the barrier height and width are crucial parameters that define the coupling strength between the QDs, via the CB and VB WFs overlaps due to tunneling to neighbor QDs. As a result with increasing coupling we see a "forest" of optical transition lines. The case of two-QDs molecule can be extended to N QDs, which leads us to the formation of minibands, as shown for the case of QW superlattices [178]. Depending on coupling strength we can distinguish three types of QDSL: SL with strong QD coupling, which is basically a system close to a QWR; completely decoupled QDs (week coupling); and system with intermediate coupling strength. Applying an electric field to a strongly coupled QDSL can be used to dynamically change the system and tune it among these categories. In particular, an electric filed can remove the degeneracy of the CB and VB states, resulting in the so-called Wannier–Stark ladder effect [179].

We have simulated pyramidal QDSL structures where the coupling strength is significant enough to produce SL minibands. The model is an extension of the QDM system (see figure 6). In the first example (low barrier case description). The QDSL is sandwiched between external barriers of 40% nominal Al content. The results for a 5-QDSL structure with these parameters are displayed in figure 10. The CB states are presented in figure 10 (a), where the confinement energies of the first CB states are shown, with a schematic inset of the structure. The right side displays the calculated WFs isosurfaces. The envelope functions of the CB SL states are not completely delocalized due to the small number of coupled QDs and the strong effects of the external barriers. The VB structure, presented in figure 10 (b), is more complex due to VB mixing effects and difference effective masses. The remarkable effect is that the lower energy VB states are delocalized across

the entire SL and have dominant LH character. This is in contrast to the HH-like lowest energy VB state for the uncoupled QDs.

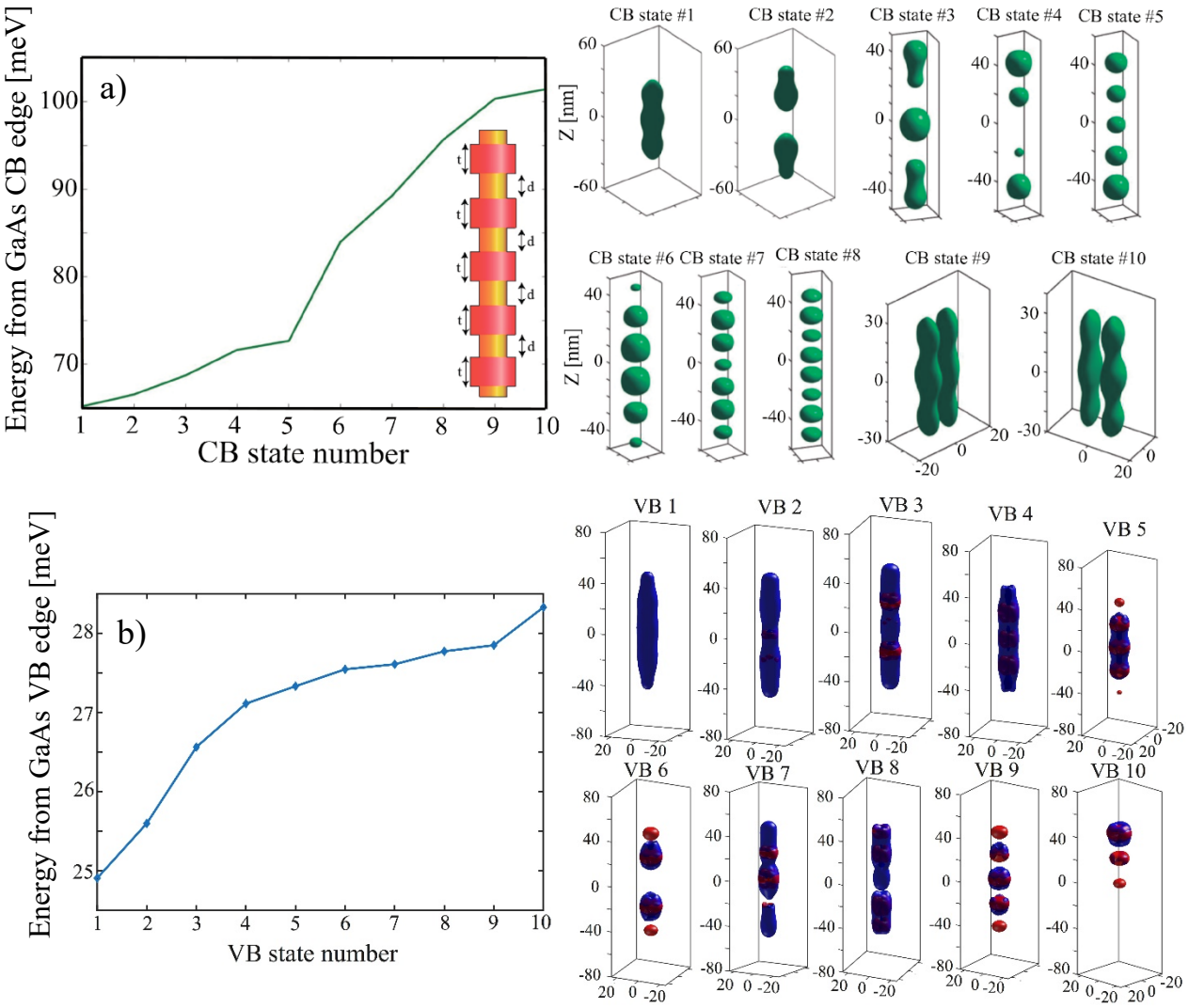

Figure 10. 5-QD pyramidal QDSL structure (see text for parameters). (a) Confinement energies of the first CB states. Inset is a schematic picture of the QDSL core part. Right panel: CB WFs (probability density isosurface) of the first 10 CB states. (b) Confinement energies of the first VB states. Right panel: VB WFs of the first 10 VB states; Red and blue colors indicate HH and LH components.

Another case considered here is a weaker coupling QDSL, presented in figure 11. In this case, 10 coupled QDs are embedded into a vertical (central) QWR with a following barrier parameters: composition is 50% nominal Al content and barrier thickness is 7 nm. This case is corresponded to strong modularity regime of the GS wavefunction. The coupled CB and VB states are now closely spaced in energy, and start forming a SL quasi-continuous minibands. The WFs consist of periodic parts (in each QD) modulated by envelope functions. Differently than in the more strongly coupled (low barrier case), the coupled VB states maintain HH character. Thus not just the effective wavefunction ratio length vs width responsible for emission polarization character but also WF shape.

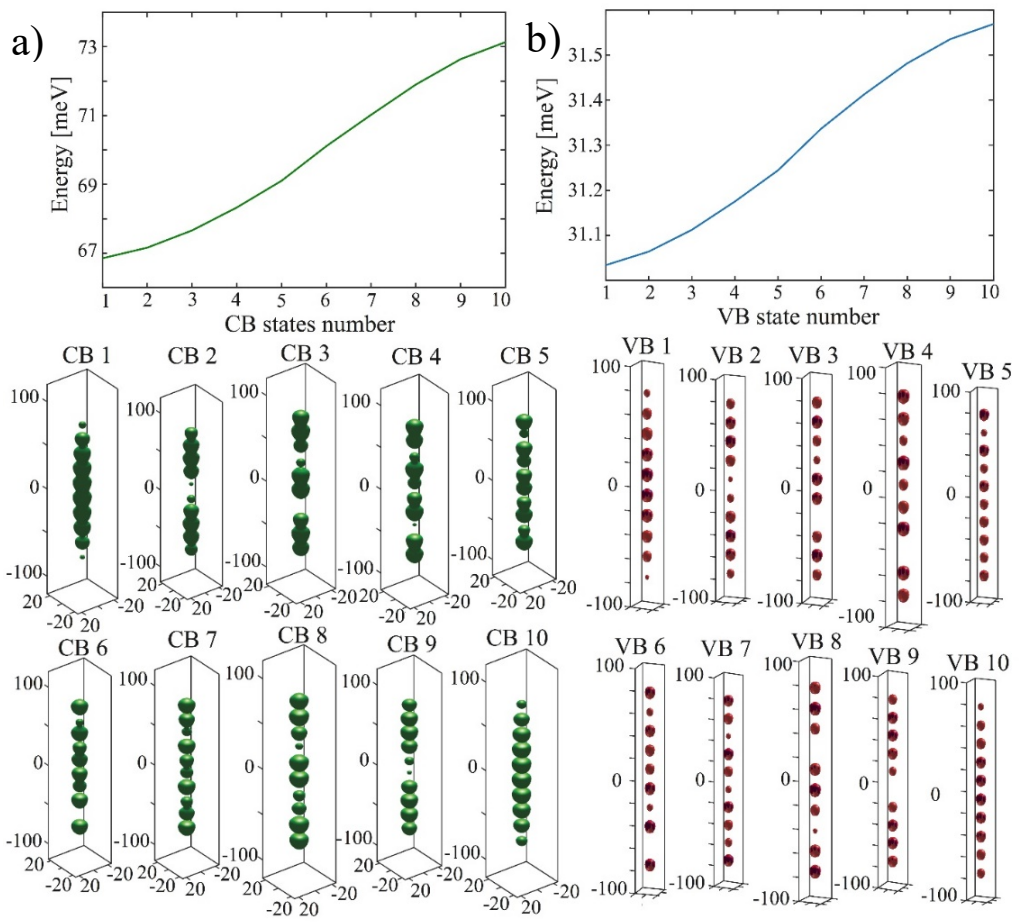

Figure 11. 10-QD pyramidal QDSL structure (see text for parameters). (a) Confinement energies and WFs (probability density isosurfaces) of the first 10 CB states. (b) Confinement energies and WFs of the first 10 VB states bellow; Red and blue colors indicate HH and LH components.

The CB and VB structure of the 10-QDs SL under electric field (1000 V/cm) is presented in figure 12. Due to the relatively high barriers between the QDs, the WFs are localized in a few QDs. The center of mass (WF) of each state is shifted on equal distance (QD to QD) from state to state (figure 12 (a)). The CB dispersion line demonstrates almost liner behavior with respect to the state number. In the VB, the electric field causes the holes to tunnel through the barriers and this leads to the formation of LH like states instead of the HH states formed in the absence of electric field (compare with figure 11).

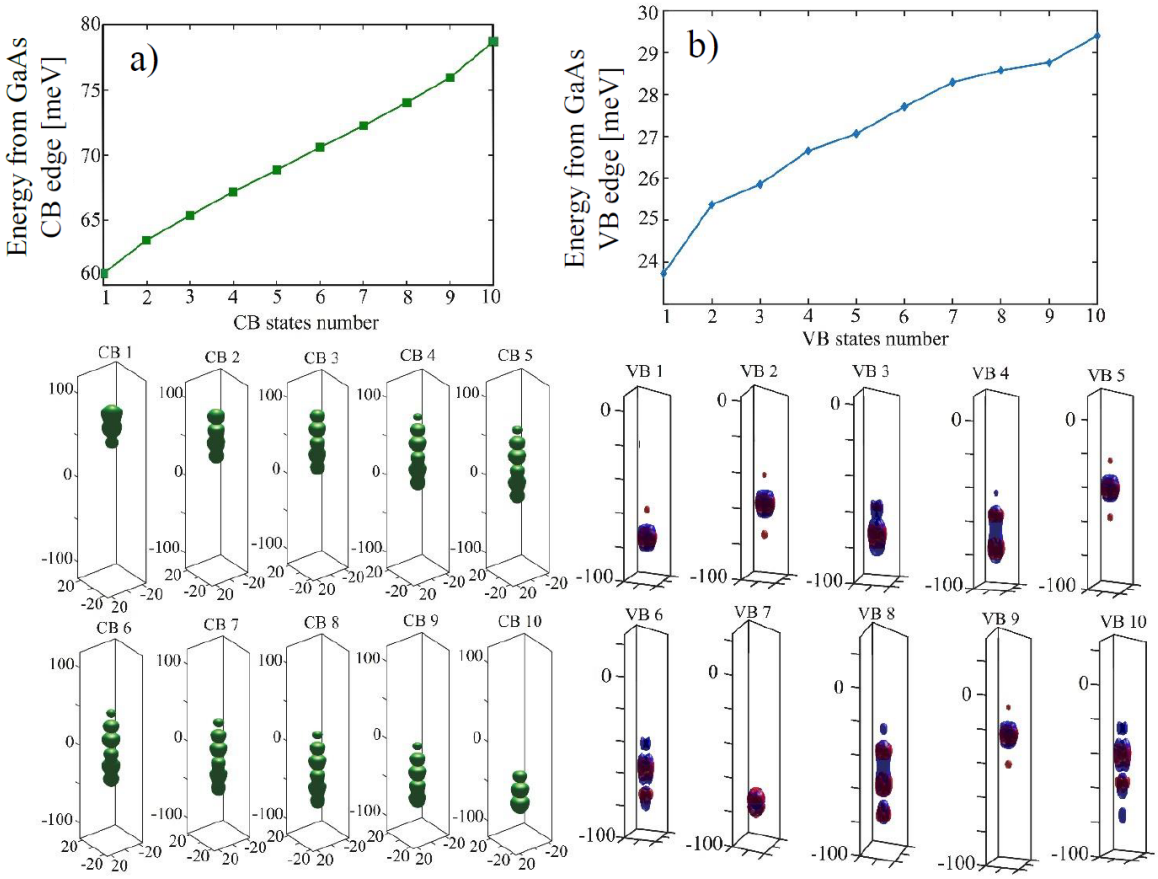

Figure 12. 10-QD pyramidal QDSL structure (see text for parameters) under electric field E=1000 [V/cm] (along z direction). (a) Confinement energies of the first CB states and CB WFs (probability density isosurface) of the first 10 CB states bellow. (b) Confinement energies of the first VB states and VB WFs of the first 10 VB states bellow; Red and blue colors indicate HH and LH VB WFs components.

The calculated spectra of the considered QDSLs (10-QDs), under electric field, are presented in figure 13. As in the QWR case, the electric field causes localization of the CB and VB states in different parts of the SL. The result is reduced overlaps between the low energy states of the CB and the VB, and the optical spectra consist predominantly of transitions between exited states. In particular, the effect of the electric field is to qualitatively change the polarization features of the weakly coupled QD SL. Their spectra now show a forest of mixed HH/LH lines as opposed to almost pure HH transitions in the absence of the electric field.

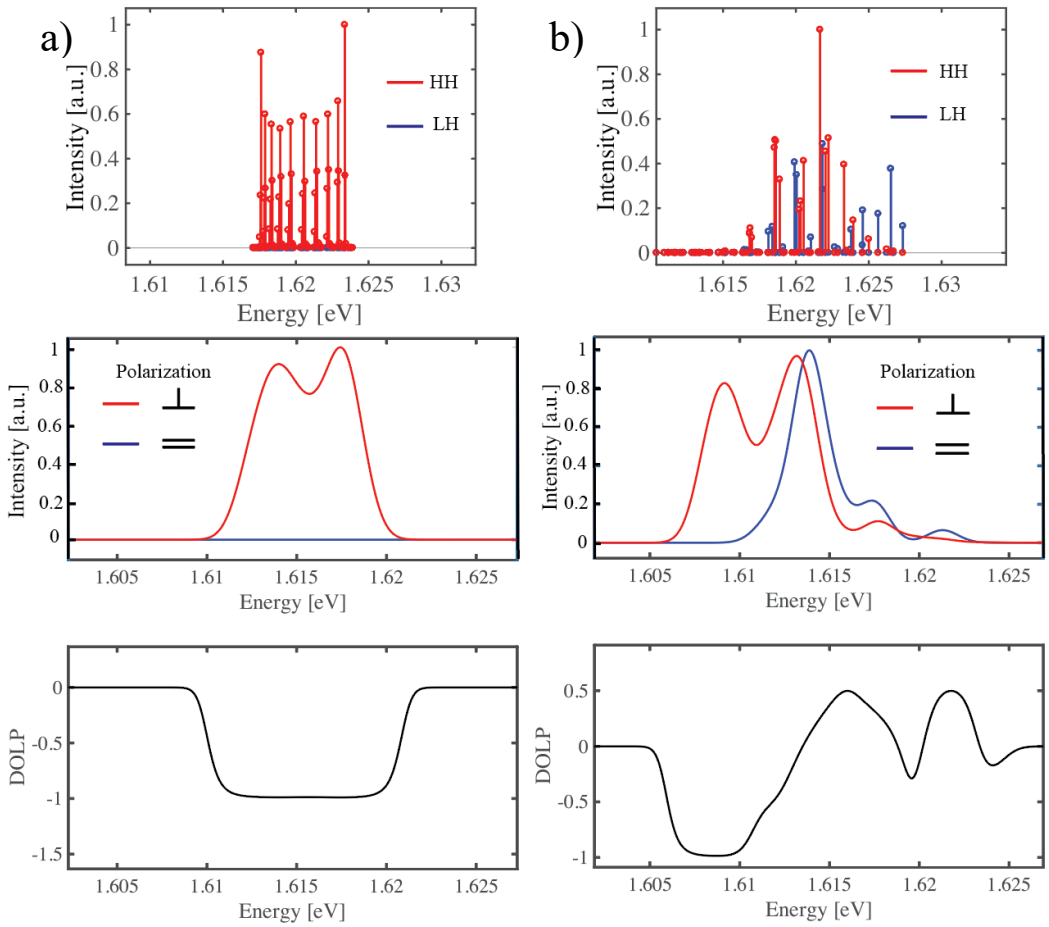

Figure 13. Left side (a) SL 10 QD spectra, spectra with coulomb interaction, DOLP. Right side (b) SL 10 QD AlGaAs under electric field 0.1 mV/nm, spectra, spectra with coulomb interaction, DOLP.

4. Conclusion

The sensitivity of VB state structure to the environment of QD and QDM makes them good candidates for polarization controlled single photon source. To find a good structural parameters for polarization switching a number of QDs was simulated from 8 nm and 23 nm length. The “equilibrium” point where LH and HH are at the same energy positions was found in between 12-14 nm long QD. Application of electric field along the QD change the VB structure in such that GS of VB becomes HH thus DOLP changes. QDM nanostructure is more sensitive to the potential variations in the barrier between the QDs and the physical principle of polarization switching effect relay on coupling strength between the QDs. High sensitivity of QDM VB structure to the coupling strength environmental parameters makes them useful as polarization switching device. External electric field modifies the coupling strength between QDs, thus affects on DOLP. This knowledge will be useful for construction of future polarization switching devices. We went further and increased the number of coupled QD up to 5 and 10 to investigate different coupling regimes and its effect on GS VB in QDSL. It appears that despite of the fact that GS WF was long as LH state in QWRs but because of its strong modularity by high internal potential berries between QDs. Effect of optical miniband formation in QD SL and the effect of electric field was discussed.

5. References

[1] K. W. J. Barnham *et al.*, "Quantum well solar cells," *Phys. E Low-Dimensional Syst. Nanostructures*, vol. 14, no. 1–2, pp. 27–36, 2002, doi: 10.1016/S1386-9477(02)00356-9.

[2] S. Nakamura, M. Senoh, N. Iwasa, and S. I. Nagahama, "High-power InGaN single-quantum-well-structure blue and violet light-emitting diodes," *Appl. Phys. Lett.*, vol. 67, no. 1995, p. 1868, 1995, doi: 10.1063/1.114359.

[3] Z. I. Alferov, "Nobel lecture: The double heterostructure concept and its applications in physics, electronics, and technology," *Rev. Mod. Phys.*, vol. 73, no. 3, pp. 767–782, 2001, doi: 10.1103/RevModPhys.73.767.

[4] B. F. Levine, "Quantum-well infrared photodetectors," *J. Appl. Phys.*, vol. 74, no. 8, 1993, doi: 10.1063/1.354252.

[5] E. O. Kane, "Band structure of indium antimonide," *J. Phys. Chem. Solids*, vol. 1, no. 4, pp. 249–261, 1957, doi: 10.1016/0022-3697(57)90013-6.

[6] S. L. Chuang, N. Peyghambarian, and S. Koch, " Physics of Optoelectronic Devices ," *Phys. Today*, vol. 49, no. 7, pp. 62–62, 1996, doi: 10.1063/1.2807693.

[7] I. Vurgaftman, J. R. Meyer, and L. R. Ram-Mohan, "Band parameters for III-V compound semiconductors and their alloys," *J. Appl. Phys.*, vol. 89, no. 11 I, pp. 5815–5875, 2001, doi: 10.1063/1.1368156.

[8] R. J. Warburton *et al.*, "Coulomb interactions in small charge-tunable quantum dots: A simple model," *Phys. Rev. B*, vol. 58, no. 24, pp. 16221–16231, 1998, doi: 10.1103/PhysRevB.58.16221.

[9] R. F. Kopf, M. H. Herman, M. L. Schnoes, A. P. Perley, G. Livescu, and M. Ohring, "Band offset determination in analog graded parabolic and triangular quantum wells of GaAs/AlGaAs and GaInAs/AlInAs," *J. Appl. Phys.*, vol. 71, no. 10, pp. 5004–5011, 1992, doi: 10.1063/1.350600.

[10] W. Langbein, H. Gislason, and J. M. Hvam, "Optimization of the confinement energy of quantum-wire states in T-shaped GaAs/Al(x)Ga(1-x)As structures," *Phys. Rev. B*, vol. 54, no. 20, pp. 14595–14603, 1996, doi: 10.1103/PhysRevB.54.14595.